PHYSICAL REVIEW B **86**, 121102(R) (2012)

Topological insulator phase in halide perovskite structures

Hosub Jin,* Jino Im,† and Arthur J. Freeman
Department of Physics and Astronomy, Northwestern University, Evanston, Illinois 60208, USA
(Received 2 April 2012; revised manuscript received 26 July 2012; published 10 September 2012)

Topological insulators are a novel quantum state of matter that reveals their properties and shows exotic phenomena when combined with other phases. Hence, priority has been given to making a good quality topological insulator interface with other compounds. From the applications point of view, the topological insulator phase in perovskite structures could be important to provide the various heterostructure interfaces with multifunctional properties. Here, by performing a tight-binding analysis and first-principles calculations, we predict that cubic-based $CsPbI_3$ and $CsSnI_3$ perovskite compounds under reasonable hydrostatic pressure are feasible candidates for three-dimensional topological insulators. Combined with cubic symmetry, the spin and total angular momentum doublets forming the valence and conduction bands result in a prototype of a continuum model, representing three-dimensional isotropic Dirac fermions, and govern the topological phase transition in halide perovskite materials.

DOI: 10.1103/PhysRevB.86.121102 PACS number(s): 71.20.−b, 73.20.At

Ever since it was first suggested and the topologically nontrivial insulating phase[1–4] was found, much effort has been made to find new topological insulator (TI) materials because of their novelty as a new quantum state of matter important in both fundamental physics and for electronic and spintronic device applications. Not only TI itself, but also the combination with other phases, including trivial band insulators, superconductors, and magnetic materials, show interesting phenomena such as Majorana fermions,[5] giant magnetoelectric effects,[6] topological excitons,[7] quantum anomalous Hall effect,[1] and image magnetic monopole;[8] these have not been shown in any other condensed matter system. The majority of TI materials predicted and/or confirmed so far is based on the hexagonal structure;[9–14] there are few examples with cubic symmetry: half-Heusler,[15–18] oxide perovskite heterostructures,[19] and antiperovskite compounds.[20] However, half-Heusler and antiperovskites need extra distortions to attain an inverted insulating gap, which makes for symmetry lowering, and the perovskite heterostructure is basically a two-dimensional (2D) TI phase based on the buckled honeycomb structure. To date, therefore, no three-dimensional (3D) TIs were found in the literally cubic phase where the highly degenerate conduction or valence band edges are easily formed due to the high symmetry.

Finding a cubic-based TI is important for offering diversity in the TI catalog. Above all, combined with state-of-the-art engineering techniques in the perovskite heterostructure field,[21,22] a cubic perovskite TI, if possible, can provide a rich variety of new interfacial phenomena by adding topological order to the existing systems. Taking into account the topologically protected surface states that merge at the boundary between trivial and nontrivial insulators, the heterostructure interface with a TI perovskite could provide a rich source where different kinds of quasiparticles interact with each other inside the confined 2D region and cooperate to show the exotic properties.

Here, we present several cubic halide perovskites as possible candidates for 3D TI materials obtained by a tight-binding (TB) analysis and density-functional theory (DFT) calculations. To capture the low energy quasiparticle spectrum in the halide perovskite series, the TB Hamiltonian is constructed by using an s- and p-orbital basis at each cubic site. After truncating the original TB Hamiltonian down to a 4×4 minimal continuum model, the topological phase transition can be properly described through 3D isotropic massive Dirac fermions; the condition for the transition is derived in terms of microscopic energy scales such as on-site potentials, hopping parameters, and spin-orbit coupling (SOC) strength. Finally, DFT calculations reveal the feasibility of this topological phase transition in $CsBI_3$ (B = Sn,Pb) compounds.

To investigate the electronic structures and topological phases, the first-principles calculations were first performed by using the full-potential linearized augmented plane wave method[23] with local density approximation (LDA) for the exchange-correlation functional. The relativistic SOC was included by a second variational procedure. For the momentum space integrations, a $9 \times 9 \times 9$ mesh of special k points was used in the 3D irreducible Brillouin zone wedge. We used a wave-vector cutoff of the basis set equal to $K_{\max} = 3.5$ a.u. and an angular momentum expansion up to $l_{\max} = 8$ for both the potential and charge density. The muffin-tin radii of Cs, Pb, Sn, and I were 2.7, 2.8, 2.7, and 2.6 a.u., respectively. We then employed the self-consistent screened-exchange LDA (sX-LDA) which provides a better energy functional for the excited states by modeling the exchange-correlation hole within a nonlocal density scheme.

In ABX_3-type perovskite structures, the A-site cation is chemically inert so that the states from cation B and anion X prevail near the Fermi level. The basic electronic structures of the $CsPbI_3$ cubic phase without SOC are shown in Fig. 1. Obviously, the conduction bands mainly consist of Pb $6p$-orbital states whose triple degeneracy is seen at the Γ and R points in the Brillouin zone. Most interestingly, at the valence band maximum, the wave function is expressed as a linear combination of Pb $6s$- and I $5p$-orbital states, following the singlet s-orbital symmetry; in other words, orbital degrees of freedom are quenched. Antibonding between Pb $6s$ and I $5p$ with strong σ character raises this state close to the Fermi level. As shown in Fig. 1(c), the parities of the basis sets constructing the valence and conduction bands are even and

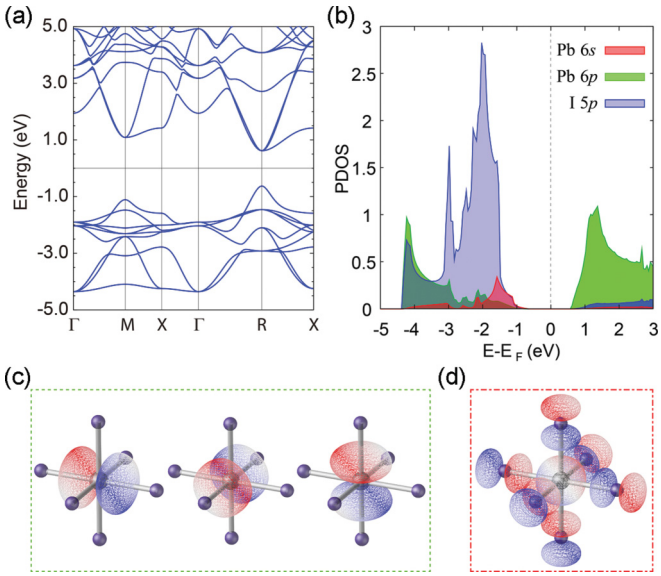

FIG. 1. (Color online) (a) Electronic band structure, (b) projected density of states of $CsPbI_3$, and the Bloch wave functions of (c) triply degenerate p bands at the conduction band minimum and (d) nondegenerate s-like band at the valence band maximum.

odd, respectively, which makes the nontrivial band topology possible by inverting and exchanging their parities.

Based on these observations, an attempt to make a clear description of the band dispersion of the halide perovskite is made through constructing the TB Hamiltonian by using an s- and p-orbital basis at each cubic site as building blocks. The real space TB Hamiltonian is given by

$$\mathcal{H}_{\rm TB} = \sum_{\vec{R},\mu} \epsilon_\mu \psi^\dagger_\mu(\vec{R})\psi_\mu(\vec{R}) + \sum_{\vec{R}\vec{\eta},\mu\nu} t^{\sigma/\pi}_{\mu\nu} \psi^\dagger_\mu(\vec{R}+\vec{\eta})\psi_\nu(\vec{R}) + \sum_{\vec{R}} \lambda \vec{L}(\vec{R})\cdot\vec{s}(\vec{R}), \quad (1)$$

where $\psi^\dagger_\mu(\vec{R})$ $(\mu = 1,2,3,4)$ is an αth component of the fermion creation operator vector $\Psi^\dagger(\vec{R}) = [S^\dagger(\vec{R}), P^\dagger_x(\vec{R}), P^\dagger_y(\vec{R}), P^\dagger_z(\vec{R})]$ at cubic sites $\vec{R}$, and $\vec{\eta}$ is one of the six vectors connecting the nearest neighbor in the cubic lattice. The first term on the right hand side of Eq. (1) denotes the on-site potential of each basis, and $\epsilon_1 \equiv \epsilon_s$, $\epsilon_2 = \epsilon_3 = \epsilon_4 \equiv \epsilon_p$, where $\epsilon_s < \epsilon_p$. In the second term, we consider four different intra- and interorbital hopping integrals: t^σ_{ss}, t^σ_{pp}, t^π_{pp}, and t^σ_{sp}. The third term is the on-site SOC which plays a central role to realize the TI phase.[24] The essential feature of this Hamiltonian is the fully SOC active conduction p bands and the inactive valence s band. The valence s band is barely influenced by SOC, whereas the $|l=1\rangle \otimes |s=1/2\rangle p$ states are split into a $|j=3/2\rangle$ quartet raised by $\lambda/2$ and a $|j=1/2\rangle$ doublet lowered by $-\lambda$. Consequently, combined with the band dispersion, the $|s=1/2\rangle$ and $|j=1/2\rangle$ manifolds become the main ingredients to describe the low energy spectrum of the quasiparticle excitation around the R point, and thus govern the topological phase of the system. As a result, distinguished from other highly symmetric lattices possessing highly degenerate conduction and/or valence bands, the halide perovskites have nondegenerate conduction and valence bands except for Kramers degeneracy. They are thus suitable to realize the nontrivial band topology without extra distortions to lower the symmetry and the degeneracy.

By integrating out the $|j=3/2\rangle$ states and expanding the sinusoidal functions up to the order of k^2 where $\vec{k} \equiv \vec{K} - \vec{G}_{\rm R} = \vec{K} - (\pi,\pi,\pi)$, we can acquire the effective 4×4 continuum Hamiltonian composed of the $|s=1/2\rangle$ and $|j=1/2\rangle$ subspace in the vicinity of the R point. The reduced Hamiltonian is written as

$$\mathcal{H}_{\rm eff}(\vec{k}) = \frac{\xi_s(\vec{k})+\xi_p(\vec{k})-\lambda}{2}\tau_0\otimes\sigma_0 + \frac{\xi_s(\vec{k})-\xi_p(\vec{k})+\lambda}{2}\tau_z \otimes\sigma_0 + \frac{2}{\sqrt{3}}t^\sigma_{sp}\tau_y\otimes(\vec{k}\cdot\vec{\sigma}^*), \quad (2)$$

where

$$\xi_s(\vec{k}) = \epsilon_s + 6t^\sigma_{ss} - \left[t^\sigma_{ss} + \frac{8}{3}\frac{\left(t^\sigma_{sp}\right)^2}{\epsilon_p-\epsilon_s-2t^\sigma_{pp}-4t^\pi_{pp}-6t^\sigma_{ss}+\lambda/2}\right]k^2,$$

$$\xi_p(\vec{k}) = \epsilon_p - 2t^\sigma_{pp} - 4t^\pi_{pp} + \frac{1}{3}\left(t^\sigma_{pp}+2t^\pi_{pp}\right)k^2,$$

τ_i and σ_i are Pauli matrices denoting orbital and spin degrees of freedom, respectively, and τ_0 and σ_0 are the 2×2 unit matrix. This Hamiltonian represents a 3D massive Dirac fermion, which is an isotropic version of the continuum model introduced in the Bi_2Se_3 family.[10] The topological phase transition is directly related to the sign change in the mass of the Dirac fermion,[25] the second term in the right hand side of Eq. (2), at $\vec{k}=0$. Considering that $\Delta\epsilon \equiv \epsilon_p - \epsilon_s$ and every hopping parameter is positive, the condition for the TI phase is simply written as $\epsilon_s + 6t^\sigma_{ss} > \epsilon_p - 2t^\sigma_{pp} - 4t^\pi_{pp} - \lambda$. By noticing that $2t^\sigma_{pp} + 4t^\pi_{pp}$ and $6t^\sigma_{ss}$ correspond to half of the conduction and valence bandwidth, W_p and W_s, respectively, the above nontrivial condition is rewritten as

$$\frac{W_s+W_p}{2} + \lambda > \Delta\epsilon; \quad (3)$$

the summation of the half bandwidth of the conduction and valence bands and SOC splitting exceeds the on-site potential difference. (See Fig. 2.) The nontrivial condition in Eq. (3) contains every microscopic energy scale used in the TB Hamiltonian except for t^σ_{sp} because it does not participate in determining the energy levels at the R point. However, unless t^σ_{sp} has a nonzero value, the conduction and valence bands are independent, and show semimetallic behavior even under the nontrivial condition.

According to the bulk-boundary correspondence, the Fermi level crosses an odd number of surface states. The existence of the topologically protected surface states at the nontrivial condition can also elucidate the TI phase of the system described by the TB Hamiltonian. Figure 3 presents the TB electronic band structures of the bulk and (001) surface geometries under the three different conditions: trivial, critical, and nontrivial cases. For the trivial case $[(W_s+W_p)/2+\lambda < \Delta\epsilon]$, both the bulk and surface have band gaps. For the critical case $[(W_s+W_p)/2+\lambda = \Delta\epsilon]$, the conduction and valence bands touch each other at the R point, and form a 3D

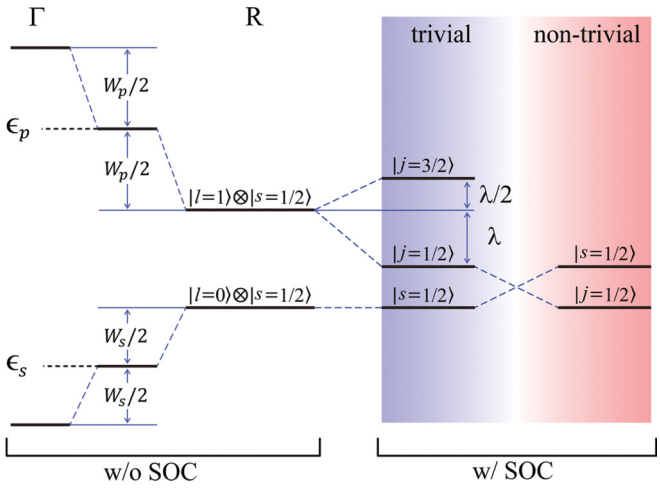

FIG. 2. (Color online) Schematic diagram of the basic electronic structure of the cubic halide perovskite series. Combined with the band dispersion and SOC, total angular momentum doublets ($j = 1/2$) and spin doublets ($s = 1/2$) are formed at the conduction band bottom and valence band top, respectively. With a successive operation of the hydrostatic pressure, the conduction and valence bands are inverted, and the system becomes TI.

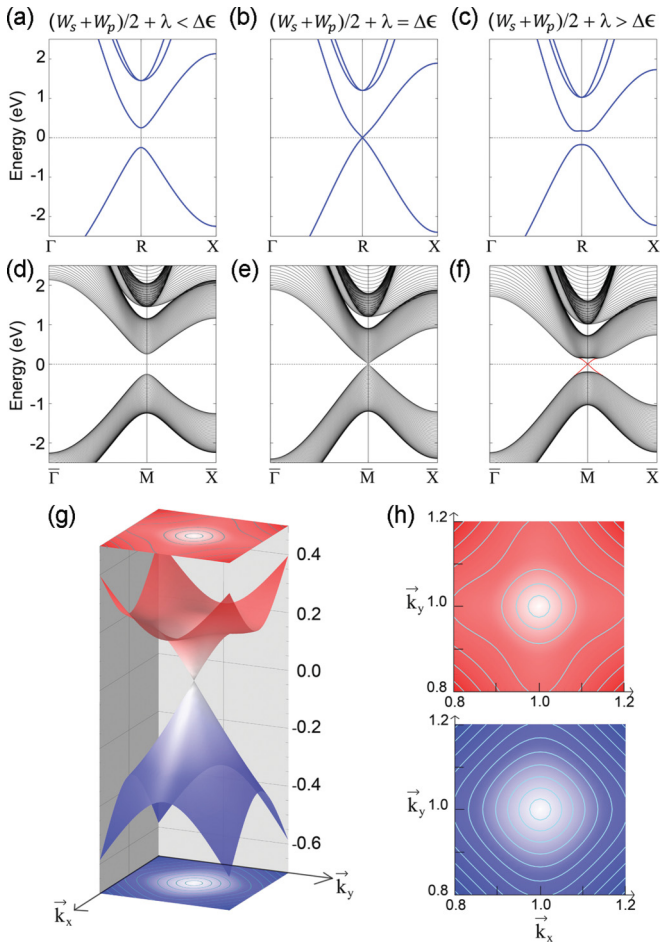

FIG. 3. (Color online) TB band structures of (a)–(c) bulk and (d)–(f) 51-layer slab geometry with (0,0,1) surface under the trivial [(a), (d)], critical [(b), (e)], and nontrivial conditions [(c), (f)], respectively. The topologically protected surface states are shown in (f); (g) and (h) show their 3D plot and an isoenergy contour map with a 0.04 eV interval.

isotropic massless Weyl fermion in the bulk band structure, as predicted in the effective continuum model in Eq. (2). The surface electronic structure also shows gapless continuum bands originating from the bulk semimetallic band structure. Finally, under the nontrivial condition, as a result of the band inversion between the $|s = 1/2\rangle$ and $|j = 1/2\rangle$ states, a single gapless surface state emerges at around the $\overline{M}$ point in the surface Brillouin zone, while there remains a bulk band gap, which is a typical characteristic of the strong 3D TI. Figures 3(g) and 3(h) depict the 3D plot of the gapless surface state shown in Fig. 3(f), and its isoenergy contour map. Near the Dirac point of the surface state, circular cross sections are shown, whereas the warping effect arises away from the Dirac point. The warping effect is a direct consequence of the fourfold symmetry of the cubic crystal, and thus appears as a rectangular shape in the isoenergy cross section[26,27] [cf. Fig. 3(h)].

Recalling the effective continuum model and the nontrivial condition in Eqs. (2) and (3), the TI phase is accessible when the large hopping parameters and the large SOC strength are available. For the purpose of realizing the nontrivial phase in the ABX_3 halide perovskite structures, heavy elements should be chosen for the B and X sites; heavy elements at the B site are essential to acquire the large SOC strength which fully splits the conduction p bands at the R point, and heavy halogens at the X site can support the large hopping parameters. The extended nature of the halogen outermost p orbitals plays an important role by mediating the intra- and interorbital hopping process, even though they do not appear explicitly in the minimal TB Hamiltonian. Following the above strategy, $CsPbI_3$ and $CsSnI_3$ are the most probable candidates for the cubic TI materials. By using the DFT method within LDA scheme, $CsPbI_3$ ($CsSnI_3$) are found to have a trivial (nontrivial) band gap of 0.020 eV (0.134 eV) at the R point. Although $CsPbI_3$ is a trivial band insulator, the band gap is quite small, which means that $(W_s + W_p)/2 + \lambda$ is slightly smaller than $\Delta\epsilon$ and the system is close to the transition point. Therefore, if we increase the left hand side of Eq. (3), the system can change its topology from a trivial to a nontrivial one. Here, we use the hydrostatic pressure to decrease the lattice constants, expecting an increase in the bandwidth. As a result, a 0.5% reduction from its experimental lattice constant makes $CsPbI_3$ have a nontrivial band topology with a 0.023 eV band gap (Fig. 4(a)).

At this point, it is appropriate to emphasize the incorrectness in the band gap estimation by employing the LDA scheme—a well-known problem—which could also prevent predicting the correct topological phase of the materials under investigation. The underestimation of the band gap effectively denotes the lessening of $\Delta\epsilon$ in terms of the parameters used in the TB Hamiltonian, which is directly linked to the overestimation of the nontrivial topological phase. Now, sX-LDA is known to provide a better description of the excited states and band gaps,[28] Hence, we adopted the advanced sX-LDA method to find the band gap as well as the band topology more accurately. With the gap corrections, $CsPbI_3$ and $CsSnI_3$ turn out to show

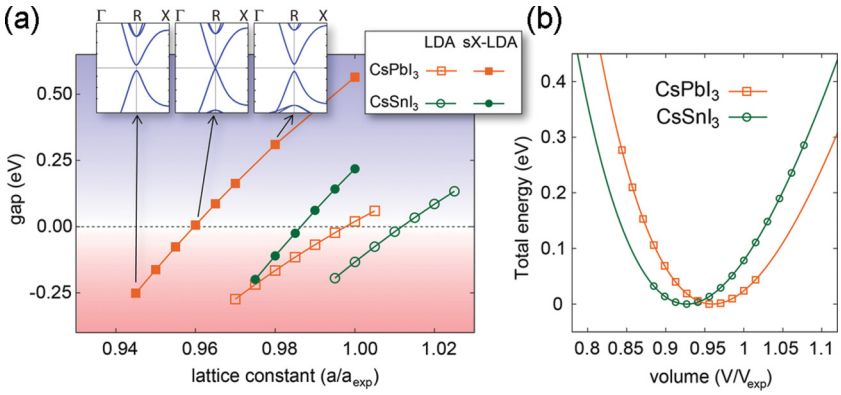

FIG. 4. (Color online) (a) The band gap dependence on the lattice constants, and (b) the total energy as a function of the unit-cell volume in $CsPbI_3$ and $CsSnI_3$. Open rectangles and circles denote LDA and solid ones correspond to the gap corrected sX-LDA results. The positive gap values indicate the trivial phase, whereas the negative means nontrivial.

trivial band gaps of 0.566 and 0.218 eV, respectively. Even though both materials belong to the trivial band insulators, the small band gaps again imply that these compounds are located in the vicinity of the topological phase boundary, and are able to be tuned to the TI phase under a reasonable amount of hydrostatic pressure. With decreasing lattice constants, $CsPbI_3$ and $CsSnI_3$ enter into the TI phase at a 4.04% and 1.36% reduction, respectively, resulting from the increment of the bandwidth. By fitting the total energy as a function of the unit-cell volume as shown in Fig. 4(b), the bulk moduli B_0 of $CsPbI_3$ and $CsSnI_3$ are estimated to be 19.88 and 20.84 GPa in LDA, and the critical pressures to make the systems nontrivial are 3.33 and 0.96 GPa,[14] respectively, which are easily achievable in experiments.

It is worthwhile to remark on the low symmetric phases in the halide perovskite series. The cubic phase in $CsPbI_3$ and $CsSnI_3$ is stable only at high temperature, and the lower symmetric phases appear as the temperature decreases. $CsSnI_3$, for example, undergoes two structural phase transitions upon lowering the temperature: cubic to tetragonal, and finally to the orthorhombic phase. The symmetry lowering induced by distortions of SnI_6 octahedra makes an extra splitting in the threefold degenerate p states. However, the small splitting is overwhelmed by the larger SOC strength, and the $|j = 1/2\rangle$ states are still robust at the conduction band edge. Therefore, the low energy electronic band structure, composed of the $|s = 1/2\rangle$ and $|j = 1/2\rangle$ states in the cubic phase, are nearly unaffected by the symmetry lowering distortions, and so is the band topology.[24] Considering the lattice distortion as a small perturbation, the continuum model in Eq. (2) might be modified to represent anisotropic Dirac fermions.

In conclusion, we have investigated the possibility of the nontrivial insulating phase in several halide perovskites by both the microscopic TB Hamiltonian and the more realistic DFT calculations within the sX-LDA scheme. Their most prominent feature is that the crystal structure has the highest symmetry, but the electronic structure has the simplest valence and conduction bands made up of the nondegenerate s and split-off p bands. As a consequence, the low energy spectrum is designated as 3D isotropic massive Dirac fermions, and the mass term easily changes its sign under reasonable hydrostatic pressure.

Once combined with advanced experimental techniquess in the atomic-scale synthesis of the artificial heterostructures, the perovskite 3D TI can provide a novel platform for diverse potential applications by introducing a new degree of freedom, the so-called topological order. The surface state protected by time-reversal symmetry is a new player in this heterostructure interface field, whose encounter with old players such as superconductivity, magnetism, ferroelectricity, orbital ordering, and so on might be a source of new physics.

Support from the US DOE under Grant No. DE-FG02-88ER45372 is gratefully acknowledged.

*h-jin@northwestern.edu
†j-im@northwestern.edu

[1] F. D. M. Haldane, Phys. Rev. Lett. **61**, 2015 (1988).
[2] C. L. Kane and E. J. Mele, Phys. Rev. Lett. **95**, 146802 (2005).
[3] B. A. Bernevig, T. L. Hughes, and S.-C. Zhang, Science **314**, 1757 (2006).
[4] M. König *et al.*, Science **318**, 766 (2007).
[5] L. Fu and C. L. Kane, Phys. Rev. Lett. **100**, 096407 (2008).
[6] X.-L. Qi, T. L. Hughes, and S.-C. Zhang, Phys. Rev. B **78**, 195424 (2008).
[7] B. Seradjeh, J. E. Moore, and M. Franz, Phys. Rev. Lett. **103**, 066402 (2009).
[8] X.-L. Qi, R. Li, J. Zang, and S.-C. Zhang, Science **323**, 1184 (2009).
[9] Y. Xia *et al.*, Nat. Phys. **5**, 398 (2009).
[10] H. Zhang *et al.*, Nat. Phys. **5**, 438 (2009).
[11] B. Yan *et al.*, Europhys. Lett. **90**, 37002 (2010).
[12] H. Jin, J.-H. Song, A. J. Freeman, and M. G. Kanatzidis, Phys. Rev. B **83**, 041202 (2011).
[13] S. V. Eremeev *et al.*, Nat. Commun. **3**, 635 (2012).
[14] M. Bahramy, B.-J. Yang, R. Arita, and N. Nagaosa, Nat. Commun. **3**, 679 (2012).
[15] S. Chadov *et al.*, Nat. Mater. **9**, 541 (2010).
[16] H. Lin *et al.*, Nat. Mater. **9**, 546 (2010).
[17] D. Xiao, Y. Yao, W. Feng, J. Wen, W. Zhu, X. Q. Chen, G. M. Stocks, and Z. Zhang, Phys. Rev. Lett. **105**, 096404 (2010).
[18] X. Dai, T. L. Hughes, X.-L. Qi, Z. Fang, and S.-C. Zhang, Phys. Rev. B **77**, 125319 (2008).

[19]D. Xiao, W. Zhu, Y. Ran, N. Nagaosa, and S. Okamoto, Nat. Commun. **2**, 596 (2011).
[20]Y. Sun, X.-Q. Chen, S. Yunoki, D. Li, and Y. Li, Phys. Rev. Lett. **105**, 216406 (2010).
[21]J. Mannhart and D. G. Schlom, Science **327**, 1607 (2010).
[22]H. Y. Hwang *et al*., Nat. Mater. **11**, 103 (2012).
[23]E. Wimmer, H. Krakauer, M. Weinert, and A. J. Freeman, Phys. Rev. B **24**, 864 (1981).
[24]See Supplemental Material at http://link.aps.org/supplemental/10.1103/PhysRevB.86.121102 for details on the TB Hamiltonian and the electronic band structures of $CsSnI_3$ with different symmetries.
[25]X.-L. Qi and S.-C. Zhang, Phys. Today **63**(1), 33 (2010).
[26]Y. L. Chen *et al*., Science **325**, 178 (2009).
[27]L. Fu, Phys. Rev. Lett. **103**, 266801 (2009).
[28]D. M. Bylander and L. Kleinman, Phys. Rev. B **41**, 7868 (1990).